Study of the effect of the tensor correlation in oxygen isotopes with the charge- and parity-projected Hartree-Fock method

Satoru Sugimoto*
Kyoto University, Kitashirakawa, Kyoto 606-8502, Japan

Kiyomi Ikeda†
The Institute of Physical and Chemical Research (RIKEN), Wako, Saitama 351-0198, Japan

Hiroshi Toki‡
Research Center for Nuclear Physics (RCNP), Osaka University, Ibaraki, Osaka 567-0047, Japan
(Received 21 July 2006; published 25 January 2007)

Recently, we developed a mean-field-type framework that treats the correlation induced by the tensor force. We treat the tensor correlation by introducing intrinsic single-particle states with parity and charge mixing. We make a total wave function with definite charge number and good parity by performing the charge number and parity projections. Taking a variation of the total energy calculated with the projected wave function, we obtain a Hartree-Fock-like equation (charge- and parity-projected Hartree-Fock equation). We extend further the charge- and parity-projected Hartree-Fock method to include a three-body force, which is important to reproduce the saturation property of nuclei in a mean-field framework. We apply the charge- and parity-projected Hartree-Fock method to sub-closed-shell oxygen isotopes (^{14}O, ^{16}O, ^{22}O, ^{24}O, and ^{28}O) to study the effect of the tensor correlation and its dependence on neutron number. We obtain reasonable binding energies and matter radii for these nuclei. It is found that relatively large energy gains come from the tensor force in these isotopes and further the blocking effect on the tensor correlation arises due to additional neutrons.

DOI: 10.1103/PhysRevC.75.014317 PACS number(s): 21.60.Jz, 21.10.Dr

I. INTRODUCTION

The tensor force plays important roles in nuclear structure. The study of nuclear matter with the Brueckner theory showed that the tensor force has a large effect on the binding mechanism and provides the saturation property of nuclear matter [1]. The variational calculations with very large model space exhibit a large attractive energy comes from the tensor force [2,3]. The tensor force seems to be responsible for about a half of the single-particle spin-orbit splitting in light nuclei [4–6].

Recently due to the development of experimental techniques, we have an access to various kinds of unstable nuclei experimentally. Those experiments reveal that the shell structures of unstable nuclei may change from those of stable nuclei [7,8]. Considering the importance of the tensor force in nuclear structure, the tensor force probably has an effect on such structure changes of nuclei [9]. Therefore, the study of the effect of the tensor force in neutron-rich nuclei is very important.

To study the effect of the tensor force in medium and heavy mass regions in the nuclear chart, including unstable nuclei, we developed a theoretical framework based on a mean-field-type model [10–13]. One of the most important tensor correlation in closed-shell nuclei is expressed in two-particle–two-hole ($2p2h$) configuration mixing. In a usual Hartree-Fock calculation, the $2p2h$ correlation induced by the tensor force cannot be treated properly. The effect of the tensor force is thought to be included effectively in other kinds of forces like the central, LS, and density-dependent forces in the usual Hartree-Fock calculations. To treat the tensor force explicitly, we introduce intrinsic single-particle states with parity and charge mixing considering the pseudoscalar and isovector characters of the pion, which mediates the tensor force [10,11]. Because the total wave function made of such single-particle states with parity and charge mixing does not have a good parity and a definite charge number, we perform the parity and charge number projections before variation [12,13]. We call this method the charge- and parity-projected Hartree-Fock (CPPHF) method. In the previous studies we applied the CPPHF method to the α particle and showed that the tensor correlation can be treated in the CPPHF method. The CPPHF method was also applied to ^{8}Be to study the effect of the tensor force on α clustering [14].

There are other attempts to treat the tensor correlation by expanding usual model spaces like a mean-field model [15], a shell model [6], and antisymmetrized molecular dynamics (AMD) [16]. Those studies, including ours, showed the importance of the $2p2h$ configuration mixing and high-momentum components in single-particle states, which are not treated in usual model-space calculations. Neff and his collaborators took a different approach to treat the tensor correlation [17]. They used the unitary correlation operator method (UCOM) to make an effective interaction in a moderate model space. In their effective interaction, the attractive correlation by the tensor force is included in other forces like the central and LS forces. They performed the calculations up to the second-order

*Electronic address: satoru@ruby.scphys.kyoto-u.ac.jp
†Electronic address: k-ikeda@riken.jp
‡Electronic address: toki@rcnp.osaka-u.ac.jp

perturbation based on Hartree-Fock calculations using their effective interaction and obtained a nice reproduction of binding energies over the whole mass region [18]. Otsuka and his collaborators [9] showed that a particle-hole (ph) correlation by the tensor force is also important and changes single-particle spin-orbit splittings of neutron (proton) orbits with proton (neutron) numbers. This effect of the tensor force was discussed in Hartree-Fock calculations in the literature [19,20].

In the present article, we apply the CPPHF method to sub-closed-shell oxygen isotopes, ^{14}O, ^{16}O, ^{22}O, ^{24}O, and ^{28}O, which are assumed to have sub-closed-shell structures for neutron orbits up to $0p_{3/2}$, $0p_{1/2}$, $0d_{5/2}$, $1s_{1/2}$, and $0d_{3/2}$ respectively, to see the dependence of the correlation induced by the tensor force on neutron number. We extend the CPPHF method to treat a three-body force, which is needed to reproduce the saturation property of nuclei with large mass numbers. In Sec. II we explain the CPPHF method with a three-body force. In Sec. III the results of the CPPHF method are presented. In Sec. IV we summarize the article.

II. CHARGE- AND PARITY-PROJECTED HARTREE-FOCK METHOD WITH A THREE-BODY FORCE

In this section we formulate the CPPHF method in the case where a three-body force exists. A Hamiltonian for an A-body system with two-body and three-body forces can be written as

$$\hat{H} = \sum_{a=1}^{A} \hat{t}(x_a) + \sum_{a>b=1}^{A} \hat{v}^{(2)}(x_a, x_b) + \sum_{a>b>c=1}^{A} \hat{v}^{(3)}(x_a, x_b, x_c), \tag{1}$$

where $\hat{t}$, $\hat{v}^{(2)}$, and $\hat{v}^{(3)}$ are one-body, two-body, and three-body operators, respectively. x's are coordinates that include spin and isospin. In the CPPHF method, we assume as single-particle states the ones with parity and charge mixing. It means each single-particle wave function has both positive-parity and negative-parity components and both proton and neutron components. The single-particle wave function that consists of these four components has the following form,

$$\psi_\alpha(x) = \sum_{p_\alpha=\pm} \sum_{t_{z\alpha}=\pm 1/2} \psi_{p_\alpha, t_{z\alpha}}(x). \tag{2}$$

In the above equation, p_α denotes parities, $+$ for positive parity and $-$ for negative parity, and $t_{z\alpha}$ denotes isospins, $+1/2$ for proton and $-1/2$ for neutron. In the CPPHF method, we take as a wave function of an A-body system a Slater determinant that consists of the single-particle states with parity and charge mixing,

$$\Psi^{\text{intr}} = \frac{1}{\sqrt{A!}} \hat{\mathcal{A}} \prod_{a=1}^{A} \psi_{\alpha_a}(x_a). \tag{3}$$

Here, $\hat{\mathcal{A}}$ is the antisymmetrization operator. Because Ψ^{intr} does not have a good parity and a definite charge number, we need to perform the projection operators of parity ($\pm$) and charge number (Z) on Ψ^{intr} to obtain the wave function with a good parity and a definite charge number;

$$\Psi^{(\pm;Z)} = \hat{\mathcal{P}}^{\text{p}}(\pm)\hat{\mathcal{P}}^{\text{c}}(Z)\Psi^{\text{intr}}. \tag{4}$$

Here, $\hat{\mathcal{P}}^{\text{p}}(\pm)$ is the parity-projection operator, where $\hat{\mathcal{P}}^{\text{p}}(+)$ projects out a positive-parity state and $\hat{\mathcal{P}}^{\text{p}}(-)$ projects out a negative-parity one. $\hat{\mathcal{P}}^{\text{c}}(Z)$ is the charge-number-projection operator, which projects out a wave function with a charge number Z. Therefore, $\Psi^{(\pm;Z)}$ has a good parity ($\pm$) and a definite charge number (Z). The parity projection operator $\hat{\mathcal{P}}^{\text{p}}(\pm)$ is defined as

$$\hat{\mathcal{P}}^{\text{p}}(\pm) = \frac{1 \pm \hat{P}}{2} \quad \left(\hat{P} = \prod_{a=1}^{A} \hat{p}_a\right), \tag{5}$$

where the total parity operator $\hat{P}$ is the product of the parity operator $\hat{p}_a$ for each single-particle state. The charge projection operator $\hat{\mathcal{P}}^{\text{c}}(Z)$ is defined as

$$\begin{aligned}\hat{\mathcal{P}}^{\text{c}}(Z) &= \frac{1}{2\pi}\int_0^{2\pi} d\theta e^{i(\hat{Z}-Z)\theta} \\ &= \frac{1}{2\pi}\int_0^{2\pi} d\theta e^{-iZ\theta}\hat{C}(\theta) \quad \left(\hat{Z} = \sum_{a=1}^{A} \frac{1+\tau_a^3}{2}\right),\end{aligned} \tag{6}$$

where $\hat{Z}$ is the charge number operator, which is the sum of the single-particle proton projection operator $(1+\tau_a^3)/2$, and the charge-rotation operator is defined as $\hat{C}(\theta) = e^{i\hat{Z}\theta}$.

We take the expectation value for the Hamiltonian $\hat{H}$ with the projected wave function and obtain the energy functional,

$$\begin{aligned}E^{(\pm;Z)} &= \frac{\langle\Psi^{(\pm;Z)}|\hat{H}|\Psi^{(\pm;Z)}\rangle}{\langle\Psi^{(\pm;Z)}|\Psi^{(\pm;Z)}\rangle} \\ &= \frac{\langle\Psi^{\text{intr}}|\hat{H}|\hat{\mathcal{P}}^{\text{p}}(\pm)\hat{\mathcal{P}}^{\text{c}}(Z)\Psi^{\text{intr}}\rangle}{\langle\Psi^{\text{intr}}|\hat{\mathcal{P}}^{\text{p}}(\pm)\hat{\mathcal{P}}^{\text{c}}(Z)\Psi^{\text{intr}}\rangle} \\ &= \frac{\frac{1}{4\pi}\int_0^{2\pi} d\theta e^{-iZ\theta}[E^{(0)}(\theta) \pm E^{(\text{P})}(\theta)]}{\frac{1}{4\pi}\int_0^{2\pi} d\theta e^{-iZ\theta}[n^{(0)}(\theta) \pm n^{(\text{P})}(\theta)]}.\end{aligned} \tag{7}$$

The denominator in the right-hand side of the above equation is the normalization of the total wave function,

$$\begin{aligned}n^{(\pm;Z)} &\equiv \langle\Psi^{(\pm;Z)}|\Psi^{(\pm;Z)}\rangle \\ &= \frac{1}{4\pi}\int_0^{2\pi} d\theta e^{-iZ\theta}[n^{(0)}(\theta) \pm n^{(\text{P})}(\theta)].\end{aligned} \tag{8}$$

Here, $n^{(0)}(\theta)$ is the determinant of the norm matrix between the original single-particle wave functions ψ_{α_a} and the charge-rotated single-particle wave functions $\psi_{\alpha_a}(\theta)$. $n^{(\text{P})}(\theta)$ is the determinant of the norm matrix between the original single-particle wave functions ψ_{α_a} and the parity-inverted and charge-rotated single-particle wave functions $\psi^{(\text{p})}_{\alpha_a}(\theta)$.

$$\begin{aligned}n^{(0)}(\theta) &\equiv \langle\Psi^{\text{intr}}|\hat{C}(\theta)|\Psi^{\text{intr}}\rangle = \det B^{(0)}(\theta) \\ \left[B^{(0)}(\theta)_{ab} \equiv \left\langle\psi_{\alpha_a}\middle|\psi_{\alpha_b}(\theta)\right\rangle\right], \\ n^{(\text{P})}(\theta) &\equiv \langle\Psi^{\text{intr}}|\hat{P}\hat{C}(\theta)|\Psi^{\text{intr}}\rangle = \det B^{(\text{P})}(\theta) \\ \left[B^{(\text{P})}(\theta)_{ab} \equiv \left\langle\psi_{\alpha_a}\middle|\psi^{(\text{p})}_{\alpha_b}(\theta)\right\rangle\right].\end{aligned} \tag{9}$$

The charge-rotated wave function $\psi_{\alpha_a}(x_b;\theta)$ and the parity-inverted and charge-rotated wave function $\psi^{(\text{p})}_{\alpha_a}(x_b;\theta)$ are

defined as

$$\begin{aligned}\psi_{\alpha_a}(x_b;\theta) &\equiv e^{i\theta(1+\tau_b^3)/2}\psi_{\alpha_a}(x_b)\\ &= e^{i\theta}\psi_{p_\alpha=+,t_{z\alpha}=1/2}(x_b)+e^{i\theta}\psi_{p_\alpha=-,t_{z\alpha}=1/2}(x_b)\\ &\quad+\psi_{p_\alpha=+,t_{z\alpha}=-1/2}(x_b)+\psi_{p_\alpha=-,t_{z\alpha}=-1/2}(x_b),\end{aligned} \tag{10}$$

$$\begin{aligned}\psi^{(\mathrm{p})}_{\alpha_a}(x_b;\theta) &\equiv \hat{p}_b e^{i\theta(1+\tau_b^3)/2}\psi_{\alpha_a}(x_b)\\ &= e^{i\theta}\psi_{p_\alpha=+,t_{z\alpha}=1/2}(x_b)-e^{i\theta}\psi_{p_\alpha=-,t_{z\alpha}=1/2}(x_b)\\ &\quad+\psi_{p_\alpha=+,t_{z\alpha}=-1/2}(x_b)-\psi_{p_\alpha=-,t_{z\alpha}=-1/2}(x_b),\end{aligned} \tag{11}$$

where $\hat{p}_b$ is the single-particle parity operator in Eq. (5) and $(1+\tau_b^3)/2$ is the single-particle proton projection operator in Eq. (6).

The numerator in the right-hand side of Eq. (7) is the unnormalized total energy,

$$\langle\Psi^{(\pm;Z)}|\hat{H}|\Psi^{(\pm;Z)}\rangle \equiv \frac{1}{4\pi}\int_0^{2\pi} d\theta e^{-iZ\theta}[E^{(0)}(\theta)\pm E^{(\mathrm{P})}(\theta)]. \tag{12}$$

$E^{(0)}(\theta)$ in the right-hand side of Eq. (12) has a similar form as a simple Hartree-Fock energy but the single-particle wave functions in the ket are modified by the charge rotation,

$$\begin{aligned}E^{(0)}(\theta) &\equiv \left\langle\Psi^{\mathrm{intr}}\middle|\hat{H}\hat{C}(\theta)\middle|\Psi^{\mathrm{intr}}\right\rangle\\ &= \sum_{a=1}^{A}\left\langle\psi_{\alpha_a}\middle|\hat{t}\middle|\tilde{\psi}_{\alpha_a}(\theta)\right\rangle\\ &\quad+\sum_{a>b=1}^{A}\left\langle\psi_{\alpha_a}\psi_{\alpha_b}\middle|\hat{v}^{(2)}\middle|\tilde{\psi}_{\alpha_a}(\theta)\widehat{\tilde{\psi}}_{\alpha_b}(\theta)\right\rangle\\ &\quad+\sum_{a>b>c=1}^{A}\left\langle\psi_{\alpha_a}\psi_{\alpha_b}\psi_{\alpha_c}\middle|\hat{v}^{(3)}\middle|\tilde{\psi}_{\alpha_a}(\theta)\widehat{\tilde{\psi}_{\alpha_b}(\theta)\tilde{\psi}_{\alpha_c}}(\theta)\right\rangle.\end{aligned} \tag{13}$$

Here, $\tilde{\psi}_{\alpha_a}(x;\theta)$ is the superposition of $\psi_{\alpha_a}(x;\theta)$ weighted by the inverse of the charge-rotated norm matrix $[B^{(0)}(\theta)^{-1}]_{ba}$,

$$\tilde{\psi}_{\alpha_a}(x;\theta)=\sum_{b=1}^{A}\psi_{\alpha_b}(x;\theta)[B^{(0)}(\theta)^{-1}]_{ba}. \tag{14}$$

This summation for $\psi_{\alpha_b}(x;\theta)$ comes from the antisymmetrization of the total wave function. The hats in the last two terms represent the antisymmetrization as

$$\left|\tilde{\psi}_{\alpha_a}(\theta)\widehat{\tilde{\psi}}_{\alpha_b}(\theta)\right\rangle = \left|\tilde{\psi}_{\alpha_a}(\theta)\tilde{\psi}_{\alpha_b}(\theta)-\tilde{\psi}_{\alpha_b}(\theta)\tilde{\psi}_{\alpha_a}(\theta)\right\rangle, \tag{15}$$

$$\begin{aligned}\left|\tilde{\psi}_{\alpha_a}(\theta)\widehat{\tilde{\psi}_{\alpha_b}(\theta)\tilde{\psi}_{\alpha_c}}(\theta)\right\rangle &= \left|\tilde{\psi}_{\alpha_a}(\theta)\tilde{\psi}_{\alpha_b}(\theta)\tilde{\psi}_{\alpha_c}(\theta)\right.\\ &\quad+\tilde{\psi}_{\alpha_b}(\theta)\tilde{\psi}_{\alpha_c}(\theta)\tilde{\psi}_{\alpha_a}(\theta)\\ &\quad+\tilde{\psi}_{\alpha_c}(\theta)\tilde{\psi}_{\alpha_a}(\theta)\tilde{\psi}_{\alpha_b}(\theta)\\ &\quad-\tilde{\psi}_{\alpha_a}(\theta)\tilde{\psi}_{\alpha_c}(\theta)\tilde{\psi}_{\alpha_b}(\theta)\\ &\quad-\tilde{\psi}_{\alpha_c}(\theta)\tilde{\psi}_{\alpha_b}(\theta)\tilde{\psi}_{\alpha_a}(\theta)\\ &\quad\left.-\tilde{\psi}_{\alpha_b}(\theta)\tilde{\psi}_{\alpha_a}(\theta)\tilde{\psi}_{\alpha_c}(\theta)\right\rangle.\end{aligned} \tag{16}$$

$E^{(0)}(\theta=0)$ reduces to a simple Hartree-Fock energy. $E^{(\mathrm{P})}(\theta)$ in the right-hand side of Eq. (12) has a similar form as $E^{(0)}(\theta)$ but $\tilde{\psi}_{\alpha_a}(\theta)$'s are replaced by $\tilde{\psi}^{(\mathrm{p})}_{\alpha_a}(\theta)$'s,

$$\begin{aligned}E^{(\mathrm{P})}(\theta) &\equiv \langle\Psi^{\mathrm{intr}}|\hat{H}\hat{P}\hat{C}(\theta)|\Psi^{\mathrm{intr}}\rangle\\ &= \sum_{a=1}^{A}\left\langle\psi_{\alpha_a}\middle|\hat{t}\middle|\tilde{\psi}^{(\mathrm{p})}_{\alpha_a}(\theta)\right\rangle\\ &\quad+\sum_{a>b=1}^{A}\left\langle\psi_{\alpha_a}\psi_{\alpha_b}\middle|\hat{v}\middle|\tilde{\psi}^{(\mathrm{p})}_{\alpha_a}(\theta)\widehat{\tilde{\psi}}^{(\mathrm{p})}_{\alpha_b}(\theta)\right\rangle\\ &\quad+\sum_{a>b>c=1}^{A}\left\langle\psi_{\alpha_a}\psi_{\alpha_b}\psi_{\alpha_c}\middle|\hat{v}\middle|\tilde{\psi}^{(\mathrm{p})}_{\alpha_a}(\theta)\widehat{\tilde{\psi}^{(\mathrm{p})}_{\alpha_b}(\theta)}\tilde{\psi}^{(\mathrm{p})}_{\alpha_c}(\theta)\right\rangle.\end{aligned} \tag{17}$$

Here, $\tilde{\psi}^{(\mathrm{p})}_{\alpha_a}(x;\theta)$ is the sum of $\psi^{(\mathrm{p})}_{\alpha_a}(x;\theta)$ weighted by the inverse of the parity-inverted and charge-rotated norm matrix $[B^{(\mathrm{P})}(\theta)^{-1}]_{ba}$,

$$\tilde{\psi}^{(\mathrm{p})}_{\alpha_a}(x;\theta)=\sum_{b=1}^{A}\psi^{(\mathrm{p})}_{\alpha_b}(x;\theta)[B^{(\mathrm{P})}(\theta)^{-1}]_{ba}. \tag{18}$$

We then take the variation of $E^{(\pm;Z)}$ with respect to a single-particle wave function ψ_{α_a},

$$\frac{\delta}{\delta\psi^{\dagger}_{\alpha_a}(x_a)}\left\{E^{(\pm;Z)}-\sum_{b,c=1}^{A}\epsilon_{bc}\langle\psi_{\alpha_b}|\psi_{\alpha_c}\rangle\right\}=0. \tag{19}$$

The Lagrange multiplier ϵ_{ab} is introduced to guarantee the ortho-normalization of single-particle wave functions, $\langle\psi_{\alpha_a}|\psi_{\alpha_b}\rangle=\delta_{\alpha_a,\alpha_b}$. As the result, we obtain the following Hartree-Fock-like equation with the charge and parity projections (the CPPHF equation) for each ψ_{α_a},

$$\begin{aligned}&\frac{1}{4\pi}\int_0^{2\pi}d\theta e^{-iZ\theta}\left(n^{(0)}(\theta)\left\{[\hat{h}^{(1)}(x_a;\theta)+\hat{h}^{(2)}(x_a;\theta)\right.\right.\\ &\quad+\hat{h}^{(3)}(x_a;\theta)]\tilde{\psi}_{\alpha_a}(x_a;\theta)-[E^{(\pm;Z)}-E^{(0)}(\theta)]\tilde{\psi}_{\alpha_a}(x_a;\theta)\\ &\quad\left.-\sum_{b=1}^{A}\eta^{(0)}_{ba}(\theta)\tilde{\psi}_{\alpha_b}(x_a;\theta)\right\}\pm n^{(\mathrm{P})}(\theta)\left\{[\hat{h}^{(1)(\mathrm{p})}(x_a;\theta)\right.\\ &\quad+\hat{h}^{(2)(\mathrm{p})}(x_a;\theta)+\hat{h}^{(3)(\mathrm{p})}(x_a;\theta)]\\ &\quad-[E^{(\pm;Z)}-E^{(\mathrm{P})}(\theta)]\tilde{\psi}^{(\mathrm{p})}_{\alpha_a}(x_a;\theta)\\ &\quad\left.\left.-\sum_{b=1}^{A}\eta^{(\mathrm{P})}_{ba}(\theta)\tilde{\psi}^{(\mathrm{p})}_{\alpha_b}(x_a;\theta)\right\}\right)=n^{(\pm;Z)}\sum_{b=1}^{A}\epsilon_{ab}\psi_{\alpha_b}(x_a),\end{aligned} \tag{20}$$

where $a=1,2,\ldots,A$. Here, $\eta^{(0)}_{ab}(\theta)$ and $\eta^{(\mathrm{P})}_{ab}(\theta)$ are defined as follows

$$\begin{aligned}\eta^{(0)}_{ab}(\theta) &\equiv \left\langle\psi_{\alpha_a}\middle|\hat{t}\middle|\tilde{\psi}_{\alpha_b}(\theta)\right\rangle+\sum_{c=1}^{A}\left\langle\psi_{\alpha_a}\psi_{\alpha_c}\middle|\hat{v}^{(2)}\middle|\tilde{\psi}_{\alpha_b}(\theta)\widehat{\tilde{\psi}}_{\alpha_c}(\theta)\right\rangle\\ &\quad+\frac{1}{2}\sum_{c,d=1}^{A}\left\langle\psi_{\alpha_a}\psi_{\alpha_c}\psi_{\alpha_d}\middle|\hat{v}^{(3)}\middle|\tilde{\psi}_{\alpha_b}(\theta)\widehat{\tilde{\psi}_{\alpha_c}}(\theta)\tilde{\psi}_{\alpha_d}(\theta)\right\rangle,\end{aligned} \tag{21}$$

$$\eta^{(\mathrm{P})}_{ab}(\theta) \equiv \langle\psi_{\alpha_a}|\hat{t}|\tilde{\psi}^{(\mathrm{p})}_{\alpha_b}(\theta)\rangle + \sum_{c=1}^{A}\langle\psi_{\alpha_a}\psi_{\alpha_c}|\hat{v}^{(2)}|\tilde{\psi}^{(\mathrm{p})}_{\alpha_b}(\theta)\widehat{\tilde{\psi}^{(\mathrm{p})}_{\alpha_c}}(\theta)\rangle + \frac{1}{2}\sum_{c,d=1}^{A}\langle\psi_{\alpha_a}\psi_{\alpha_c}\psi_{\alpha_d}|\hat{v}^{(3)}|\tilde{\psi}^{(\mathrm{p})}_{\alpha_b}(\theta)\widehat{\tilde{\psi}^{(\mathrm{p})}_{\alpha_c}}(\theta)\tilde{\psi}^{(\mathrm{p})}_{\alpha_d}(\theta)\rangle. \quad (22)$$

$\hat{h}^{(1)}$, $\hat{h}^{(2)}$, and $\hat{h}^{(3)}$ are the single-particle operators originated from the one-body, two-body, and three-body operators, which are defined as follows

$$\hat{h}^{(1)}\tilde{\psi}_{\alpha_a}(x_a;\theta) \equiv \hat{t}(x_a)\tilde{\psi}_{\alpha_a}(x_a;\theta), \quad (23)$$

$$\hat{h}^{(2)}\tilde{\psi}_{\alpha_a}(x_a;\theta) \equiv \sum_{b=1}^{A}\{\langle\psi_{\alpha_b}|\hat{v}^{(2)}(x_a)|\tilde{\psi}_{\alpha_b}(\theta)\rangle_1\tilde{\psi}_{\alpha_a}(x_a;\theta) - \langle\psi_{\alpha_b}|\hat{v}^{(2)}(x_a)|\tilde{\psi}_{\alpha_a}(\theta)\rangle_1\tilde{\psi}_{\alpha_b}(x_a;\theta)\}, \quad (24)$$

$$\hat{h}^{(3)}\tilde{\psi}_{\alpha_a}(x_a;\theta) \equiv \frac{1}{2}\sum_{b,c=1}^{A}\{\langle\psi_{\alpha_b}\psi_{\alpha_c}|\hat{v}^{(3)}(x_a)|\tilde{\psi}_{\alpha_b}(\theta)\widehat{\tilde{\psi}_{\alpha_c}}(\theta)\rangle_{1,2}\times\tilde{\psi}_{\alpha_a}(x_a;\theta) + \langle\psi_{\alpha_b}\psi_{\alpha_c}|\hat{v}^{(3)}(x_a)\times|\tilde{\psi}_{\alpha_c}(\theta)\widehat{\tilde{\psi}_{\alpha_a}}(\theta)\rangle_{1,2}\tilde{\psi}_{\alpha_b}(x_a;\theta) + \langle\psi_{\alpha_b}\psi_{\alpha_c}|\hat{v}^{(3)}(x_a)|\tilde{\psi}_{\alpha_a}(\theta)\widehat{\tilde{\psi}_{\alpha_b}}(\theta)\rangle_{1,2}\times\tilde{\psi}_{\alpha_c}(x_a;\theta)\}. \quad (25)$$

The expressions of $\hat{h}^{(1)(\mathrm{p})}$, $\hat{h}^{(2)(\mathrm{p})}$, and $\hat{h}^{(3)(\mathrm{p})}$ are obtained from those of $\hat{h}^{(1)}$, $\hat{h}^{(2)}$, and $\hat{h}^{(3)}$ by replacing $\tilde{\psi}_\alpha(x,\theta)$ with $\tilde{\psi}^{(\mathrm{p})}_\alpha(x,\theta)$. The notation for the integration of the two-body matrix elements,

$$\langle\psi_{\alpha_b}|\hat{v}^{(2)}(x_a)|\psi_{\alpha_c}\rangle_1 = \int dx_1\psi^\dagger_{\alpha_b}(x_1)\hat{v}^{(2)}(x_a,x_1)\psi_{\alpha_c}(x_1), \quad (26)$$

and that of the three-body matrix elements,

$$\langle\psi_{\alpha_b}\psi_{\alpha_c}|\hat{v}^{(3)}(x_a)|\psi_{\alpha_d}\psi_{\alpha_e}\rangle_{1,2} = \int dx_1\int dx_2\psi^\dagger_{\alpha_b}(x_1)\psi^\dagger_{\alpha_c}(x_2)\times\hat{v}^{(3)}(x_a,x_1,x_2)\psi_{\alpha_d}(x_1)\times\psi_{\alpha_e}(x_2) \quad (27)$$

are introduced. The system of the coupled Eqs. (20) for $a = 1,\cdots,A$ are solved self-consistently.

We give here the expressions for the expectation value of the kinetic energy $\langle\hat{T}\rangle^{(\pm;\mathrm{Z})}$ with the center-of-mass correction, that of the two-body potential energy $\langle\hat{v}^{(2)}\rangle^{(\pm;\mathrm{Z})}$, and that of three-body potential energy $\langle\hat{v}^{(3)}\rangle^{(\pm;\mathrm{Z})}$.

$$\langle\hat{T}\rangle^{(\pm;\mathrm{Z})} = \frac{1}{4\pi n^{(\pm;\mathrm{Z})}}\int_0^{2\pi}d\theta e^{-i\mathrm{Z}\theta}\left[n^{(0)}(\theta)\times\left\{\sum_{a=1}^{A}\langle\psi_{\alpha_a}|\hat{t}|\tilde{\psi}_{\alpha_a}(\theta)\rangle + \sum_{a>b=1}^{A}\langle\psi_{\alpha_a}\psi_{\alpha_b}|\times\frac{\hbar^2}{AM}\nabla_a\cdot\nabla_b|\tilde{\psi}_{\alpha_a}(\theta)\widehat{\tilde{\psi}_{\alpha_b}}(\theta)\rangle\right\}\right.$$
$$\left.\pm n^{(\mathrm{P})}(\theta)\left\{\sum_{a=1}^{A}\langle\psi_{\alpha_a}|\hat{t}|\tilde{\psi}^{(\mathrm{p})}_{\alpha_a}(\theta)\rangle + \sum_{a>b=1}^{A}\langle\psi_{\alpha_a}\psi_{\alpha_b}|\times\frac{\hbar^2}{AM}\nabla_a\cdot\nabla_b|\tilde{\psi}^{(\mathrm{p})}_{\alpha_a}(\theta)\widehat{\tilde{\psi}^{(\mathrm{p})}_{\alpha_b}}(\theta)\rangle\right\}\right], \quad (28)$$

$$\langle\hat{v}^{(2)}\rangle^{(\pm;\mathrm{Z})} = \frac{1}{4\pi n^{(\pm;\mathrm{Z})}}\int_0^{2\pi}d\theta e^{-i\mathrm{Z}\theta}\times\sum_{a>b=1}^{A}\left[n^{(0)}(\theta)\langle\psi_{\alpha_a}\psi_{\alpha_b}|\hat{v}^{(2)}|\tilde{\psi}_{\alpha_a}(\theta)\widehat{\tilde{\psi}_{\alpha_b}}(\theta)\rangle \pm n^{(\mathrm{P})}(\theta)\langle\psi_{\alpha_a}\psi_{\alpha_b}|\hat{v}^{(2)}|\tilde{\psi}^{(\mathrm{p})}_{\alpha_a}(\theta)\widehat{\tilde{\psi}^{(\mathrm{p})}_{\alpha_b}}(\theta)\rangle\right], \quad (29)$$

$$\langle\hat{v}^{(3)}\rangle^{(\pm;\mathrm{Z})} = \frac{1}{4\pi n^{(\pm;\mathrm{Z})}}\int_0^{2\pi}d\theta e^{-i\mathrm{Z}\theta}\times\sum_{a>b>c=1}^{A}\left[n^{(0)}(\theta)\langle\psi_{\alpha_a}\psi_{\alpha_b}\psi_{\alpha_c}|\hat{v}^{(3)}\times|\tilde{\psi}_{\alpha_a}(\theta)\widehat{\tilde{\psi}_{\alpha_b}}(\theta)\tilde{\psi}_{\alpha_c}(\theta)\rangle \pm n^{(\mathrm{P})}(\theta)\langle\psi_{\alpha_a}\psi_{\alpha_b}\psi_{\alpha_c}|\times\hat{v}^{(3)}|\tilde{\psi}^{(\mathrm{p})}_{\alpha_a}(\theta)\widehat{\tilde{\psi}^{(\mathrm{p})}_{\alpha_b}}(\theta)\tilde{\psi}^{(\mathrm{p})}_{\alpha_c}(\theta)\rangle\right]. \quad (30)$$

III. APPLICATIONS TO SUB-CLOSED-SHELL OXYGEN ISOTOPES

In this section, we apply the CPPHF method formulated in the last section to the ground states of the sub-closed oxygen isotopes, ^{14}O, ^{16}O, ^{22}O, ^{24}O, and ^{28}O. The parities of these nuclei in the ground states are positive. These nuclei are assumed to have the closed-shell structure up to $0p_{1/2}$ for proton and sub-closed or closed shells up to $0p_{3/2}$ (^{14}O), $0p_{1/2}$ (^{16}O), $0d_{5/2}$ (^{22}O), $1s_{1/2}$ (^{24}O), and $0d_{3/2}$ (^{28}O) for neutron. Although ^{28}O is know to be unbound from the experiment, we calculate the nucleus to study the shell-configuration dependence of the contribution from the tensor force theoretically. We assume the spherical symmetry. In this case, only the total angular momentum j is a good quantum number of a single-particle state, because parities and charges are mixed in intrinsic single-particle states. An intrinsic wave function can be written in the following form,

$$\Psi^{\mathrm{intr}} = \hat{\mathcal{A}}\prod_{0\leqslant j\leqslant j^{\max}}\prod_{-j\leqslant m\leqslant j}\prod_{1\leqslant n_j\leqslant n_j^{\max}}\psi_{n_jjm}(x). \quad (31)$$

A single-particle wave function ψ_{n_jjm} is composed of four components, proton and positive parity, proton and negative parity, neutron and positive parity, and neutron and negative parity,

$$\psi_{n_jjm}(x) = \sum_{t_z=\pm\frac{1}{2}}\left[\phi_{n_jjl_+t_z}(r)\mathcal{Y}_{jl_+m}(\Omega)\zeta(t_z) + \phi_{n_jjl_-t_z}(r)\mathcal{Y}_{jl_-m}(\Omega)\zeta(t_z)\right]. \quad (32)$$

Here, $\mathcal{Y}_{jlm}(\Omega)$ is the eigenfunction of the total angular momentum $\boldsymbol{j} = \boldsymbol{l} + \boldsymbol{s}$, $\zeta(t_z)$ is the isospin wave function with $t_z = 1/2$ for proton and $t_z = -1/2$ for neutron. l_+ and l_- are the orbital angular momenta with positive parity and negative parity, respectively. For example, $l_+ = 0$ and $l_- = 1$

for $j = 1/2, l_+ = 2$ and $l_- = 1$ for $j = 3/2$, and so on. Equation (32) indicates that in the present calculation assuming the spherical symmetry only the correlations among the same j orbits can be treated. It is a limitation of the CPPHF method with the spherical symmetry. For the calculation of ^{16}O four single-particle states with $j = 1/2$ and two states with $j = 3/2$ are included. They correspond to $\pi s_{1/2}$, $\nu s_{1/2}$, $\pi p_{1/2}$, and $\nu p_{1/2}$ for $j = 1/2$ and $\pi p_{3/2}$ and $\nu p_{3/2}$ for $j = 3/2$. Because parities and charges are mixed in single-particle states such a classification is approximately valid. For the calculation of ^{14}O one state with $j = 1/2$ is subtracted and for the calculation of ^{22}O, ^{24}O, and ^{28}O new states with $j = 5/2$, $j = 1/2$, and $j = 3/2$ are added one by one.

In the present study we use the modified Volkov force no. 1 (MV1 force) [21] for the central force and the G3RS force [22] for the noncentral forces. The MV1 force is the modified version of the Volkov force no. 1 [23] and includes the δ-function-type three-body force,

$$\hat{v}^{(3)}(x_a, x_b, x_c) = t_3 \delta(\boldsymbol{x}_a - \boldsymbol{x}_b)\delta(\boldsymbol{x}_b - \boldsymbol{x}_c). \tag{33}$$

The Majorana parameter in the MV1 force is fixed to 0.6. The G3RS is determined from the nucleon-nucleon scattering data. The effect of the tensor force is effectively included in the MV1 force because the MV1 force is determined so as to reproduce the binding energy of ^{16}O in the absence of the tensor force. The effect of the tensor force is thought to appear in the ^{3}E channel of the central force as a medium range attraction. Therefore, we multiply the medium range attraction part in the ^{3}E channel of the central force by x_C. We also multiply the three-body-force part by x_{3B}. The δ-function-type three-body force in Eq. (33) reduces to the density-dependent two-body force, $\frac{1}{6} t_3 \rho[(\boldsymbol{x}_a + \boldsymbol{x}_b)/2][1 + P_\sigma(ab)/2]\delta(\boldsymbol{x}_a - \boldsymbol{x}_b)$, for the wave functions of even-even nuclei with time-reversal symmetry in the Hartree-Fock level [24]. P_σ is the spin-exchange operator and ρ is a single-particle density. In this case the density-dependent force only acts on the ^{3}E channel. In the MV1 force t_3 is positive and the density-dependent force has the repulsive effect on the ^{3}E channel. The LS force determined from the NN scattering data is usually weak to be used in a mean field (Hartree-Fock) calculation. Hence, we multiply the LS force by 2. In this case the strength of the LS force is comparable to those adopted in the Skyrme forces and the Gogny forces [25].

We also multiply the $\tau_1 \cdot \tau_2$ part of the tensor force a numerical factor x_T as in the previous study [12], because the CPPHF method is a mean-field-type calculation and can only take into account the correlations induced by limited couplings among single-particle states. Actually, in the spherical symmetry the $2p2h$ correlation which can be treated in the CPPHF method is like $(j_{p_1} j_{p_2} j_{h_1}^{-1} j_{h_2}^{-1})$ with $j_{p_1} = j_{h_1}$ and $j_{p_2} = j_{h_2}$. However, $2p2h$ configurations with $j_{p_1} \neq j_{h_1}$ and $j_{p_2} \neq j_{h_2}$ are also important [6,26]. Furthermore, other effects may enhance the tensor correlation as mentioned in our previous article [12]. To take into account such effects effectively, we take $x_T = 1.5$ (the strong tensor force case) in addition to $x_T = 1.0$ (the normal tensor force case). x_C and x_{3B} are determined to reproduce the binding energy and the charge radius of ^{16}O for each x_T.

We expand single-particle wave functions in the Gaussian basis as in the previous study [12]. The number of the Gaussian basis used is 10 for each orbit with the minimum range 0.5 fm and the maximum range 10 fm. The CPPHF Eq. (20) is solved by the gradient or the damped gradient method [27]. The convergence of the calculation is quite slow for the case with a large difference between a proton number (Z) and a neutron number (N) as in ^{28}O. To remedy it, the quadratic constraint potential term [28] for Z,

$$\langle \Psi^{\text{intr}} | \frac{\lambda}{2} (\hat{Z} - Z)^2 | \Psi^{\text{intr}} \rangle, \tag{34}$$

is added to the energy functional (7). The addition of the constrained potential makes the convergence faster. The value of λ is taken as 1000 MeV.

A. Results for ^{16}O

We first take ^{16}O as a typical example and show the effect of the tensor force in the CPPHF method.

In Table I the results for ^{16}O in the Hartree-Fock (HF) and the CPPHF schemes are shown. In the HF scheme we fix x_T, x_C, and x_{3B} to 1.0. In the CPPHF scheme x_C and x_{3B} are 1.025 and 1.25 for the normal tensor force ($x_T = 1.0$) case, and 1.040 and 1.55 for the strong tensor force ($x_T = 1.5$) case. The root-mean-square charge radius R_c is calculated from the proton root-mean-square radius R_p as $R_c = \sqrt{R_p^2 + 0.64}$. This prescription for R_c corresponds to the assumption of the charge radius of proton as 0.80 fm. In the HF calculation the expectation value for the potential energy from the tensor force V_T is negligibly small. If we perform the charge and parity projection before variation (the CPPHF case), V_T comes out to be a sizable value. It becomes about 10 MeV for the normal tensor force case and about 40 MeV for the strong tensor force case. This result indicates that the CPPHF method is effective to treat the correlation from the tensor force. In the CPPHF cases the kinetic energy T becomes larger than in the HF case. In the CPPHF scheme, to gain the tensor correlation energy the opposite-parity components compared to the simple shell-model picture have to be mixed into single-particle states. This mixing causes an over shell correlation and, as a result, the kinetic energy becomes larger. A similar tendency is also observed in the α-particle case [12,13].

In Figs. 1, 2, and 3 the intrinsic single-particle wave functions in ^{16}O with the strong tensor force ($x_T = 1.5$) are plotted. The wave functions plotted have proton components

TABLE I. Results for ^{16}O in the HF and CPPHF method. x_T is a numerical factor multiplied to the $\tau_1 \cdot \tau_2$ part of the tensor force. E and T are the total energy and the total kinetic energy respectively. V_C, V_{3B}, V_T, V_{LS}, and V_{Coul} are the potential energies for the central, the three-body force, the tensor force, the LS force, and the Coulomb force, respectively. Those are give in the unit of MeV. R_c is the root-mean-square charge radius in the unit of fm.

	x_T	E	T	$V_C + V_{3B} + V_{\text{Coul}}$	V_T	V_{LS}	R_c
HF	1.0	−124.1	230.0	−353.2	0.0	−0.9	2.73
CPPHF	1.0	−127.1	237.1	−351.6	−11.7	−1.0	2.73
CPPHF	1.5	−127.6	253.9	−342.2	−38.3	−1.0	2.73

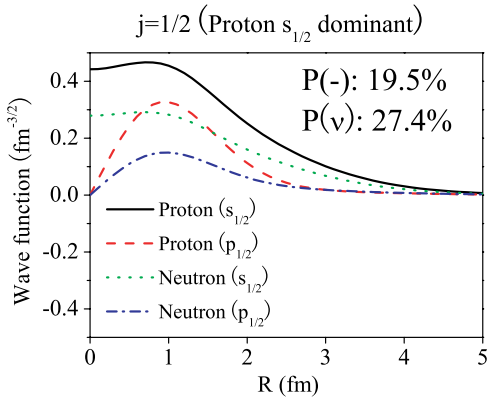

FIG. 1. (Color online) Intrinsic single-particle wave function of the $j = 1/2$ state with an $s_{1/2}$ proton component as a dominant one in ^{16}O as a function of the radial distance R. The solid, dashed, dotted, and dashed-dotted curves correspond to $s_{1/2}$ proton, $p_{1/2}$ proton, $s_{1/2}$ neutron, and $p_{1/2}$ neutron, respectively. $P(-)$ and $P(\nu)$ are the mixing probabilities of the negative-party and the neutron components, respectively.

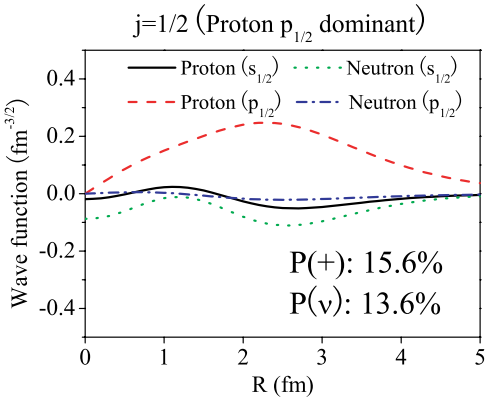

FIG. 3. (Color online) Intrinsic single-particle wave function of the $j = 1/2$ state with a $p_{1/2}$ proton component as a dominant one in ^{16}O as a function of the radial distance R. The solid, dashed, dotted, and dashed-dotted curves correspond to $s_{1/2}$ proton, $p_{1/2}$ proton, $s_{1/2}$ neutron, and $p_{1/2}$ neutron, respectively. $P(+)$ and $P(\nu)$ are the mixing probabilities of the positive-party and the neutron components, respectively.

as dominant ones. The wave function in Fig. 1 has a proton $s_{1/2}$ component as a dominant component. The mixing probabilities for negative parity ($p_{1/2}$) and neutron are 19.5 and 27.4%, respectively. From the figure you can see that the spread of the $p_{1/2}$ components are smaller than that of the $s_{1/2}$ ones. It indicates that the opposite-parity components induced by the tensor force have high-momentum components. The wave function that has a proton $p_{3/2}$ component as a dominant one is plotted in Fig. 2 and the shrinkage of $d_{3/2}$ components compared to $p_{3/2}$ ones are clearly seen also. In the wave function that has a proton $p_{1/2}$ component as a dominant one, which is plotted in Fig. 3, the shrinkage is not so clear compared to the previous two cases, probably because of the orthogonality condition on the wave function with respect to the first $j = 1/2$ state in Fig. 1.

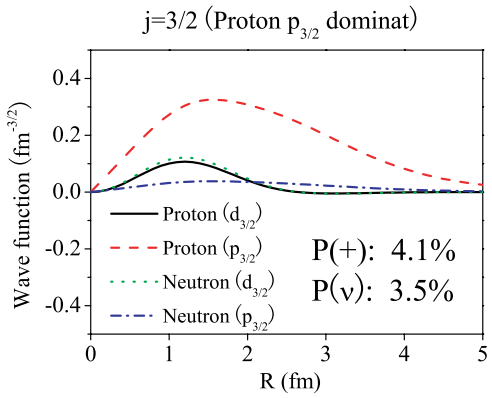

FIG. 2. (Color online) Intrinsic single-particle wave function of the $j = 3/2$ state with a $p_{3/2}$ proton component as a dominant one in ^{16}O as a function of the radial distance R. The solid, dashed, dotted and dashed-dotted curves correspond to $d_{3/2}$ proton, $p_{3/2}$ proton, $d_{3/2}$ neutron, and $p_{3/2}$ neutron, respectively. $P(+)$ and $P(\nu)$ are the mixing probabilities of the positive-party and the neutron components, respectively.

In the α-particle case, $p_{1/2}$ components mixed into $s_{1/2}$ ones are also compact in size [12,13,15]. The importance of this shrinkage is confirmed in a shell-model calculation [6] and the AMD calculation [16], too. The present result infers that the shrinkage of the opposite-parity components induced by the tensor force is generally important in heavier-mass region. There are also wave functions with a neutron component as a dominant one. The general tendency just mentioned above is almost the same if proton and neutron are interchanged.

In Fig. 4 the densities for ^{16}O in the HF and CPPHF calculations are shown. Because the tensor force induces the opposite-parity components with narrower widths in single-particle wave functions, the densities are depleted in the middle in the CPPHF calculations compared to the one in the HF calculation. This effect is larger for the case with the strong tensor force as expected. To see the effect of the tensor correlation more clearly, in Fig. 5 the charge form

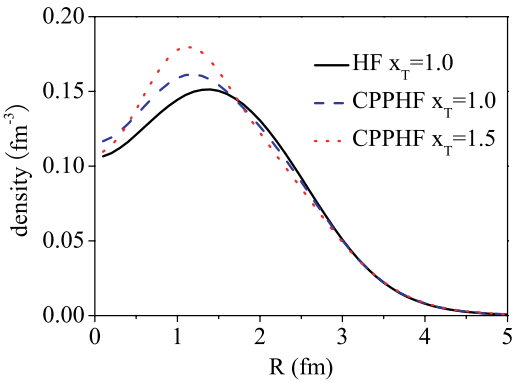

FIG. 4. (Color online) Densities for ^{16}O in the Hartree-Fock (HF) and the CPPHF methods as a function of the radial distance (R). The solid, the dashed, and the dotted curves correspond to the HF calculation, the CPPHF calculation with the normal tensor force ($x_T = 1.0$), and the CPPHF calculation with the strong tensor force ($x_T = 1.5$).

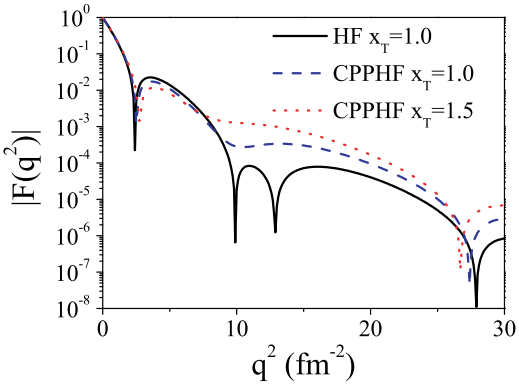

FIG. 5. (Color online) Absolute values of the charge form factor for ^{16}O in the HF and the CPPHF methods as a function of the momentum squared (q^2). The solid, the dashed, and the dotted curves correspond to the HF calculation, the CPPHF calculation with the normal tensor force ($x_T = 1.0$), and the CPPHF calculation with the strong tensor force ($x_T = 1.5$).

factors are plotted as a function of the momentum squared. From the figure, higher-momentum components appear in the CPPHF calculation. It indicates that the tensor force enhances the charge form factor in a high-momentum region. We need further investigation to compare the present result of the charge form factor in the CPPHF method with the experimental data, taking into account other correlations that cannot be treated in the present model like the short-range correlation and the meson exchange current. The enhancement of the charge form factor in a high-momentum region is also found in ^{4}He in the calculation with the charge- and parity-projected relativistic mean-field model [13].

B. Results for the oxygen isotopes

In this subsection we show the results for the sub-closed-shell oxygen isotopes.

In Fig. 6, the results for the binding energies per particle in the HF calculation (the circle symbols), the CPPHF calculation with the normal tensor force ($x_T = 1.0$) (the triangle symbols) and the CPPHF calculation with the strong tensor force ($x_T = 1.5$) (the diamond symbols) are shown. The experimental data (the square symbols) [29] are also plotted. The general tendency is reproduced in our result, although the agreement with the experimental data is not as good as the Hartree-Fock-type calculations [25,30–34]. The HF calculation with the MV1 force underestimates the binding energy of ^{14}O and ^{22}O a little bit largely. It indicates that if we adopt the central and the density-dependent forces in the recent sophisticated effective interaction, the agreement with the experimental data should become better. There is an ambiguity in the treatment of the density-dependent force when we perform the parity and charge projections, because the density-dependent force cannot be written in a simple two-body operator form. It causes a difficulty when we use the density-dependent force in the CPPHF calculation. The optimization of the central force and the management of the density-dependent force will be our future problems.

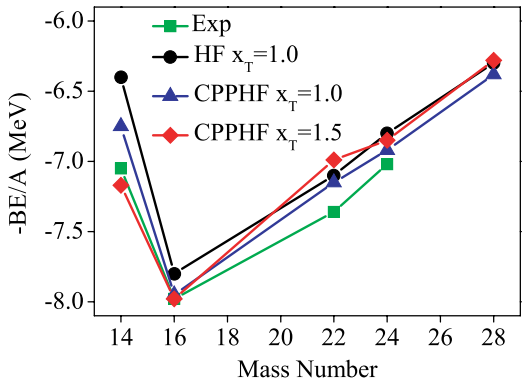

FIG. 6. (Color online) Binding energies per particle with minus sign for sub-closed-shell oxygen isotopes. The horizontal line indicates mass numbers. The circle symbols correspond to the HF calculation, the triangle ones to the CPPHF calculation with the normal tensor force ($x_T = 1.0$), and the diamond ones to the CPPHF calculation with the strong tensor force ($x_T = 1.5$). The square symbols indicate the experimental data [29].

The agreement with the experimental data is good for ^{14}O in the CPPHF method with the strong tensor force. In this case quite a large attractive potential energy comes from the tensor force as shown later.

In Fig. 7, the results for the root-mean-square matter radii (R_m) are plotted with the experimental data [30]. We use the same symbol for each case as in Fig. 6. Except for ^{14}O the results for all the three cases are almost the same and reproduce the experimental data well. For ^{14}O the CPPHF calculation with the strong tensor force gives a smaller matter radius compared to the other two calculations and the agreement with the experimental data becomes better in the strong tensor force case. The reduction of the radius is caused by the shrinkage of the opposite parity components in single-particle wave functions induced by the tensor correlation. Such an effect cannot be treated in simple Hartree-Fock calculations.

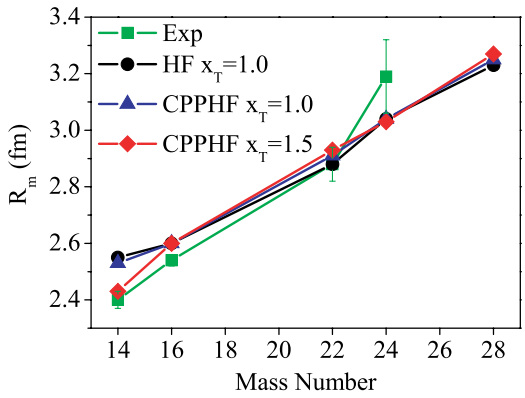

FIG. 7. (Color online) Root-mean-square matter radii for sub-closed-shell oxygen isotopes. The horizontal line indicates mass numbers. The circle symbols correspond to the HF calculation, the triangles correspond to the CPPHF calculation with the normal tensor force ($x_T = 1.0$), and the diamonds correspond to the CPPHF calculation with the strong tensor force ($x_T = 1.5$). The square symbols indicate the experimental data with error bars [30].

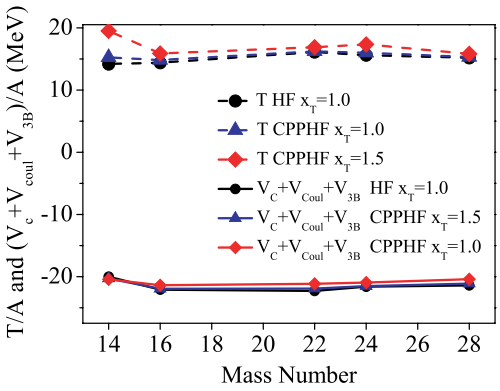

FIG. 8. (Color online) Kinetic energy (T) per particle and the sum of the potential energies from the central force V_C, the Coulomb force $V_{\rm Coul}$, and the three-body force V_{3B} divided by mass numbers. The horizontal axis indicates mass numbers. The dashed lines correspond to the kinetic energy and the solid lines to the sum of the potential energies. The circle, triangle, and diamond symbols correspond to the HF calculation, the CPPHF calculation with the normal tensor force ($x_T = 1.0$), and the CPPHF calculation with the strong tensor force ($x_T = 1.5$).

To see the effect of the tensor force on the binding mechanism in the oxygen isotopes in Fig. 8 the results for the total kinetic energy T (the dashed lines) and the sum of the potential energies from the central, the three-body and the Coulomb forces $V_C + V_{3B} + V_{\rm Coul}$ (the solid lines) are plotted. We also show in Fig. 9 the result for the potential energies from the tensor force V_T (the solid lines) and the LS force $V_{\rm LS}$ (the dashed line). The same symbols are used for the HF calculation and the CPPHF calculations with the normal and strong tensor forces as in Fig. 6. All values are divided by mass numbers to make an isotope dependence clear. The total kinetic energy and the sum of the potential energies from the central, three-body, and Coulomb forces show a volumelike behavior. The kinetic energy for ^{14}O in the CPPHF calculation with the strong tensor force is larger than the other two cases. The increase of the kinetic energy is also caused by the strong tensor correlation in ^{14}O, because to gain the correlation energy from the tensor force the opposite-parity components must be mixed into single-particle states and the opposite-parity components have larger kinetic energy.

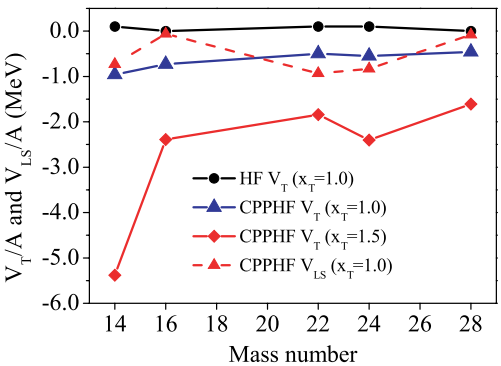

FIG. 9. (Color online) Potential energies from the tensor force (V_T) and the LS force ($V_{\rm LS}$) divided by mass numbers. The horizontal axis indicates mass numbers. The solid lines correspond to the potential energy from the tensor force. The dashed line corresponds to the potential energy from the LS force in the CPPHF calculation with the normal tensor force. The potential energies from the LS force in other cases are almost unchanged. The meanings of the symbols are the same as in Fig. 8.

The potential energies from the LS force behave in almost the same manner for the three cases. It becomes attractive if neutron shells are jj closed and negligibly small if neutron shells are LS closed. The potential energy from the tensor force becomes weakly repulsive in the HF calculation for all the oxygen isotopes. In the CPPHF calculations the potential energies from the tensor force become attractive for all the oxygen isotopes. In contrast to the LS potential energies, the tensor potential energies have sizable values in LS-closed shell nuclei like ^{16}O and ^{28}O. The attraction from the tensor force is the same order as that from the LS force even in the case with the normal tensor force. In the CPPHF case V_T becomes maximum in ^{14}O and decreases with the mass number. For the strong tensor force case, the attractive energy from the tensor force becomes larger as expected. The attractive energy is quite large for ^{14}O in the CPPHF calculation with the strong tensor force. For other isotopes the attractive energies from the tensor force are small and do not change so much with neutron number.

In Fig. 10 the probabilities of the mixing of the opposite parity components $P_{\rm mix}$ in the single-particle states with neutron components as the dominant ones are shown. It is the result of the CPPHF calculation with the normal tensor force. The result for the strong tensor force case shows almost the same tendency. In the usual shell-model classification the first $j = 1/2$ state ($s_{1/2}$ dominant), the first $j = 3/2$ state ($p_{3/2}$ dominant), the second $j = 1/2$ state ($p_{1/2}$ dominant), the first $j = 5/2$ state ($d_{5/2}$ dominant), the third $j = 1/2$ state ($s_{1/2}$ dominant), and the second $j = 3/2$ state ($d_{3/2}$

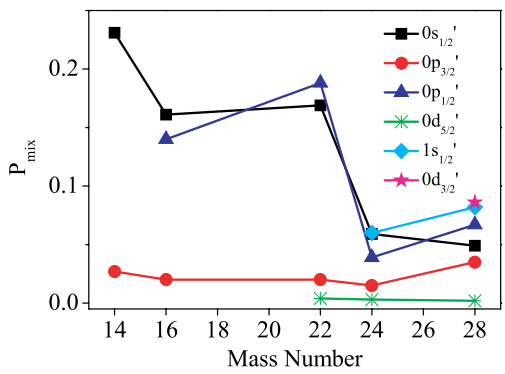

FIG. 10. (Color online) Probabilities of the mixing of the opposite-parity components for single-particle states with neutron components as dominant ones in the CPPHF calculation with the normal tensor force. The horizontal axis indicates mass numbers. The square, circle, triangle, asterisk, diamond, and star symbols correspond to the first $j = 1/2$ ($0s'_{1/2}$; $s_{1/2}$ dominant), the first $j = 3/2$ ($0p'_{3/2}$; $p_{3/2}$ dominant), the second $j = 1/2$ ($0p'_{1/2}$; $p_{1/2}$ dominant), the first $j = 5/2$ ($0d'_{5/2}$; $d_{5/2}$ dominant), the third $j = 1/2$ ($1s'_{1/2}$; $s_{1/2}$ dominant), and the second $j = 3/2$ ($0d'_{3/2}$; $d_{3/2}$ dominant), respectively.

dominant) correspond to $0s_{1/2}$, $0p_{3/2}$, $0p_{1/2}$, $0d_{5/2}$, $1s_{1/2}$, and $0d_{3/2}$, respectively. All those states are mixing states of positive and negative parities as in Eq. (32). We add a prime in the following to indicate each single-particle state has both positive-parity and negative-parity components. For example, a $0s'_{1/2}$ state has $s_{1/2}$ (positive-parity) and $p_{1/2}$ (negative-parity) components with an $s_{1/2}$ component as a dominant one. For ^{14}O the neutron orbits are filled up to $0p'_{3/2}$. The mixing probability of the opposite parity components for $0s'_{1/2}$ is larger than 20% and that for $0p'_{3/2}$ is a few percentages in ^{14}O. In the CPPHF method the tensor correlation energy is gained by parity mixing and, therefore, $P_{\rm mix}$ is a measure to indicate how each single-particle orbit contributes to the tensor correlation. The large $P_{\rm mix}$ for $0s'_{1/2}$ indicates that this orbit is largely affected by the tensor correlation. In ^{16}O, the neutron $0p'_{1/2}$ orbit is added newly. The addition of the $0p'_{1/2}$ orbit reduces the parity mixing of the $0s'_{1/2}$ orbit because they have the same total angular momentum $j = 1/2$. As the result, the tensor correlation energy becomes smaller. This effect is more significant for the strong tensor force case as seen in Fig. 9. In ^{22}O the neutron $0d'_{5/2}$ orbit is filled. Because there are no $j = 5/2$ orbit below, $P_{\rm mix}$'s for the states filled already in ^{16}O do not change largely. In ^{24}O the neutron $1s'_{1/2}$ orbit is newly occupied. The occupation of $1s'_{1/2}$ reduces $P_{\rm mix}$'s for the states with $j = 1/2$, $0s'_{1/2}$ and $0p'_{1/2}$. The tensor correlation energy is enhanced, although the amount of the change is small. Finally, in ^{28}O the neutron $0d'_{3/2}$ orbit is filled. $P_{\rm mix}$'s for the previously filled orbits change by this addition but the changes are not so large.

The change of $P_{\rm mix}$ as shown above indicates that the large change of the tensor correlation energy from ^{14}O to ^{16}O in the strong tensor force case is caused by the blocking effect for the $j = 1/2$ orbits. The blocking effect of this kind is shown to be important in the single-particle ls splitting in ^{5}He [6]. The effect of the blocking is less significant for the excess neutron orbits. The effect of the blocking on binding energies in neutron excess oxygen isotopes seems to be small but the blocking may affect single-particle natures or collectivity in neutron excess oxygen isotopes, because the mixing probability is affected by the blocking effect.

The negligible $P_{\rm mix}$ for the $0d'_{5/2}$ orbit indicates that this orbit does not contribute to the tensor correlation although there are no other occupied orbits that have $j = 5/2$. The main part of the tensor correlation comes from the $T = 0$ channel. Because the proton $j = 5/2$ orbit is not filled in neutron-excess oxygen isotopes, the $0d'_{5/2}$ orbit is hard to contribute to the tensor correlation and the mixing probability of it becomes small.

IV. SUMMARY

We studied the effect of the tensor force in the sub-closed-shell oxygen isotopes using the CPPHF method. We extended the CPPHF method to the cases with Hamiltonians, including three-body forces, although the extension is straightforward. In the CPPHF method the parity- and charge-number projections are performed before variation. By applying the CPPHF method to the oxygen isotopes actually, we have found that a sizable potential energy from the tensor force is obtained in the CPPHF method, whereas in the Hartree-Fock calculation quite a small potential energy from the tensor force is obtained.

We investigated ^{16}O in some detail. The correlation energy from the tensor force is about 10 MeV for the normal tensor force case and about 40 MeV for the strong tensor force case. In the strong tensor force case the strength of the $\tau_1 \cdot \tau_2$ channel in the tensor force is multiplied by 1.5. The opposite parity components induced in single-particle states by the tensor force have compact sizes as compared to the normal parity components. This indicates that for the tensor correlation high-momentum components are important. This fact is already found in the α-particle case [6,12,13,15,16]. The present result infers that the importance of the high-momentum component for the tensor correlation is valid in heavier-mass nuclei. We have also shown the density and the charge form factor calculated in the CPPHF method. The density in the CPPHF method is reduced around the center and is pulled in to the inside region. This is caused by the parity mixing and the shrinkage of single-particle wave functions of the opposite parities. The effect of the shrinkage appears in the charge form factor as a tail in a high-momentum region, because the shrinkage of the single-particle wave functions induces high-momentum components in the density.

In the results for the oxygen isotopes, the general tendencies for the binding energies and the matter radii are reproduced in the CPPHF calculation with the effective interaction adopted here, whereas the agreement of the binding energy with the experimental data is not so good compared to the Hartree-Fock-type calculations with recent effective interactions. The root-mean-square matter radii are well reproduced within error bars except for ^{14}O with both the normal tensor force and the strong tensor force. In the strong tensor force case, the matter radius of ^{14}O becomes smaller and close to the experimental data. The reduction of the matter radius in ^{14}O with the strong tensor force is due to the shrinkage of single-particle wave function by the strong tensor correlation, which is quite large in ^{14}O. Because the $0p_{1/2}$ neutron orbit is not occupied in ^{14}O, there are no blocking states for the $0s_{1/2}$ proton orbit and, therefore, the tensor correlation becomes large. Actually, the correlation energy from the tensor force per particle amounts to more than 5 MeV in this case. For all the oxygen isotopes the calculated potential energy from the tensor force is in the same order as that from the LS force for the normal tensor force case. In the strong tensor force case it becomes about two times larger. In contrast to the potential energy from the LS force, the potential energy from the tensor force in an LS-closed-shell nucleus does not become close to zero in the CPPHF calculation. In the Hartree-Fock calculation it becomes negligibly small because both the total spin and the total orbital angular momenta are almost zero in an LS-closed-shell nucleus. The sudden decrease of the potential energy from the tensor force from ^{14}O to ^{16}O is attributed to the blocking effect of the $j = 1/2$ orbits. The blocking effect is also seen in the neutron-excess oxygen isotopes but does not affect the binding energy largely.

In the present study we have applied the CPPHF method to the ground states of the sub-closed-shell oxygen isotopes. The application to odd-mass nuclei and open-shell nuclei to study the effect of the tensor force on single-particle natures

and the change of collectivity by the tensor correlation in a neutron excess region are interesting because the tensor force changes the spin, the orbital angular momenta and the isospin of nucleon orbits simultaneously. Such correlations can be treated in the CPPHF method by the parity and charge mixing. As for an effective interaction, we combine the available effective interaction and the tensor force in the free space with some modifications. We need to use effective interactions that have the connection with the realistic nuclear forces to reveal the relation between nuclear structure and the underlying nuclear force and have the consistency between the tensor force and other forces like the central and LS forces. The study in such a direction is also important and now under progress.

ACKNOWLEDGMENTS

We acknowledge fruitful discussions with Professor H. Horiuchi on the role of the tensor force in light nuclei. This work is supported by the Grant-in-Aid for the 21st Century COE "Center for Diversity and Universality in Physics" from the Ministry of Education, Culture, Sports, Science and Technology (MEXT) of Japan. This work is partially performed in the Research Project for the Study of Unstable Nuclei from Nuclear Cluster Aspects sponsored by the Institute of Physical and Chemical Research (RIKEN) and a part of the calculation of the present study was performed on the RIKEN Super Combined Cluster System (RSCC).

[1] H. A. Bethe, Annu. Rev. Nucl. Sci. **21**, 93 (1971).
[2] Y. Akaishi, in *Cluster Models and Other Topics*, edited by T. T. S. Kuo and E. Osnes (World Scientific, Singapore, 1986), p. 259.
[3] H. Kamada, A. Nogga, W. Glöckle, E. Hiyama, M. Kamimura, K. Varga, Y. Suzuki, M. Viviani, A. Kievsky, S. Rosati, J. Carlson, S. C. Pieper, R. B. Wiringa, P. Navrátil, B. R. Barrett, N. Barnea, W. Leidemann, and G. Orlandini, Phys. Rev. C **64**, 044001 (2001).
[4] S. Takagi, W. Watari, and M. Yasuno, Prog. Theor. Phys. **22**, 549 (1959); T. Terasawa, *ibid.* **23**, 87 (1960); A. Arima and T. Terasawa, *ibid.* **23**, 115 (1960).
[5] K. Andō and H. Bandō, Prog. Theor. Phys. **66**, 227 (1980).
[6] T. Myo, K. Katō, and K. Ikeda, Prog. Theor. Phys. **113**, 763 (2005).
[7] A. Ozawa, T. Kobayashi, T. Suzuki, K. Yoshida, and I. Tanihata, Phys. Rev. Lett. **84**, 5493 (2000).
[8] H. Grawe, Springer Lecture Notes Phys. **651**, 33 (2004).
[9] T. Otsuka, T. Suzuki, R. Fujimoto, H. Grawe, and Y. Akaishi, Phys. Rev. Lett. **95**, 232502 (2005).
[10] H. Toki, S. Sugimoto, and K. Ikeda, Prog. Theor. Phys. **108**, 903 (2002).
[11] Y. Ogawa, H. Toki, S. Tamenaga, H. Shen, A. Hosaka, S. Sugimoto, and K. Ikeda, Prog. Theor. Phys. **111**, 75 (2004).
[12] S. Sugimoto, K. Ikeda, and H. Toki, Nucl. Phys. **A740**, 77 (2004).
[13] Y. Ogawa, H. Toki, S. Tamenaga, S. Sugimoto, and K. Ikeda, Phys. Rev. C **73**, 034301 (2006).
[14] S. Sugimoto, K. Ikeda, and H. Toki, nucl-th/0511087.
[15] Y. Akaishi, Nucl. Phys. **A738**, 80 (2004).
[16] A. Doté, Y. Kanada-En'yo, H. Horiuchi, Y. Akaishi, and K. Ikeda, Prog. Theor. Phys. **115**, 1069 (2006).
[17] T. Neff and H. Feldmeier, Nucl. Phys. **A713**, 311 (2004).
[18] R. Roth, P. Papakonstantinou, N. Paar, H. Hergert, T. Neff, and H. Feldmeier, Phys. Rev. C **73**, 044312 (2006).
[19] R. M. Tarbutton and K. T. R. Davies, Nucl. Phys. **A120**, 1 (1968).
[20] A. Bouyssy, J.-F. Mathiot, N. Van Giai, and S. Marcos, Phys. Rev. C **36**, 380 (1987).
[21] T. Ando, K. Ikeda, and A. Tohsaki-Suzuki, Prog. Theor. Phys. **64**, 1608 (1980).
[22] R. Tamagaki, Prog. Theor. Phys. **39**, 91 (1968).
[23] A. B. Volkov, Nucl. Phys. **74**, 33 (1965).
[24] D. Vautherin and D. M. Brink, Phys. Rev. C **5**, 626 (1972).
[25] Z. Patyk, A. Baran, J. F. Berger, J. Dechargé, J. Dobaczewski, P. Ring, and A. Sobiczewski, Phys. Rev. C **59**, 704 (1999).
[26] T. Myo, S. Sugimoto, K. Katō, H. Toki, and K. Ikeda, Prog. Theor. Phys. (to be published); nucl-th/0607059.
[27] P.-G. Reinhard, in *Computationl Nuclear Physics 1*, edited by K. Langanke, J. A. Maruhn, and S. E. Koonin (Springer-Verlag, Berlin, 1991), Chapter 2.
[28] H. Flocard, P. Quentin, A. K. Kerman, and D. Vautherin, Nucl. Phys. **A203**, 433 (1973).
[29] G. Audi, A. H. Wapstra, and C. Thibault, Nucl. Phys. **A729**, 337 (2003).
[30] A. Ozawa, T. Suzuki, and I. Tanihata, Nucl. Phys. **A693**, 32 (2001).
[31] M. Bender, P.-H. Heenen, and P.-G. Reinhard, Rev. Mod. Phys. **75**, 121 (2003) and the references therein.
[32] D. Vretenar, A. V. Afanasjev, G. A. Lalazissis, and P. Ring, Phys. Rep. **409**, 101 (2005) and the references therein.
[33] H. Nakada and M. Sato, Nucl. Phys. **A699**, 511 (2002).
[34] H. Nakada, Nucl. Phys. **A764**, 117 (2006).